THE ASTRONOMICAL JOURNAL, 120:575–582, 2000 August

EXTREMELY RED OBJECTS FROM THE *HUBBLE SPACE TELESCOPE* NICMOS PARALLEL IMAGING SURVEY

LIN YAN,[1] PATRICK J. MCCARTHY,[1] RAY J. WEYMANN,[1] MATTHEW A. MALKAN,[2] HARRY I. TEPLITZ,[3,4] LISA J. STORRIE-LOMBARDI,[1,5] MALCOLM SMITH,[6] AND ALAN DRESSLER[1]

Received 2000 January 19; accepted 2000 March 14

ABSTRACT

We present a catalog of extremely red objects (EROs) discovered using the *Hubble Space Telescope* Near Infrared Camera and Multi-Object Spectrometer (NICMOS) parallel imaging database and ground-based optical follow-up observations. Within an area of 16 arcmin^2, we detect 15 objects with $R-\mathrm{F160W} > 5$ and $\mathrm{F160W} < 21.5$. We have also obtained K-band photometry for a subset of the 15 EROs. All of the $R-\mathrm{F160W}$ selected EROs imaged at K-band have $R-K > 6$. Our objects have $\mathrm{F110W}-\mathrm{F160W}$ colors in the range 1.3–2.1, redder than the cluster elliptical galaxies at $z \sim 0.8$ and nearly 1 mag redder than the average population selected from the F160W images at the same depth. In addition, among only 22 NICMOS pointings, we detected two groups or clusters in two fields; each contains three or more EROs, suggesting that extremely red galaxies may be strongly clustered. At bright magnitudes with $\mathrm{F160W} < 19.5$, the ERO surface density is similar to what has been measured by other surveys. At the limit of our sample, $\mathrm{F160W} = 21.5$, our measured surface density is 0.94 ± 0.24 arcmin^{-2}. Excluding the two possible groups or clusters and the one apparently stellar object reduces the surface density to 0.38 ± 0.15 arcmin^{-2}.

Key words: galaxies: elliptical and lenticular, cD — galaxies: starburst

1. INTRODUCTION

Deep near-IR imaging surveys have revealed a population of extremely red objects (EROs; Elston, Rieke, & Rieke 1988; McCarthy, Persson, & West 1992; Graham & Dey 1996; Hu & Ridgeway 1994; Soifer et al. 1994; Dey, Spinrad, & Dickinson 1995; Thompson et al. 1999). The nature of the extremely red population remains unclear. As it is defined largely by a single color, primarily $R-K$, there is no certainty that it represents a uniform class of object, and it may contain contributions from galaxies, cool stars, substellar objects, or active nuclei. The precise definition of an ERO varies among the surveys and depends on the particular bandpasses employed. Most samples were defined by $R-K \gtrsim 5$–6 or $I-K \gtrsim 4$–5. The present work is based on a somewhat different color system, that defined by the *Hubble Space Telescope* (*HST*) Near Infrared Camera and Multi-Object Spectrometer (NICMOS) F160W bandpass and conventional Kron-Cousins R magnitudes. The NICMOS F160W band is similar to the Johnson H-band filter, and the $H-\mathrm{F160W}$ color term is negligible for a flat spectral energy distribution (in f_ν units) (M. Rieke 1999, private communication). Among the resolved objects there are reasonable expectations that there should exist stellar systems at redshifts such that the k-correction applied to an old or intermediate-age population will produce very red optical to near-IR colors. Alternatively even fairly modest extinction, when observed in the same redshift range, can produce very steep spectral energy distributions in the rest-frame near-UV, and there are local examples of such objects among the dusty starburst population. The central issue regarding the nature of the resolved EROs is to understand to what degree these two classes of objects contribute to the overall population.

The earliest interpretation of the colors of EROs were centered on the old stellar population hypothesis (e.g., McCarthy et al. 1991; Hu & Ridgeway 1994), and redshifts of 1–2 were inferred from their multiband photometry. Clear examples support this interpretation, such as the weak radio source LBDS 53W091, at $z = 1.55$ (Dunlop et al. 1996), and the near-IR selected object CL 0939+4713B, at $z = 1.58$ (Soifer et al. 1999), and a concentration of EROs at $z = 1.3$ (Liu et al. 2000). Graham & Dey (1996) argued that the spectral energy distribution of HR10 (Hu & Ridgeway 1994) is well matched by a dusty star-forming galaxy at $z = 1.5$. The detection of a strong submillimeter continuum from HR10 (Cimatti et al. 1998; Dey et al. 1999) provided conclusive evidence that some EROs, if not all, are dust-enshrouded starburst galaxies with inferred star formation rates of $500 - 2000\ h_{50}^{-2}\ M_\odot\ \mathrm{yr}^{-1}$at moderate redshifts ($z \sim 1$–2). Recent deep near-IR follow-up observations of the submillimeter sources detected with the SCUBA (Smail et al. 1998) have suggested that two faint submillimeter sources may also be EROs with $I-K > 6$ (Smail et al. 1999). Liu et al. have measured redshifts for several other EROs. Most of these are also in the $0.8 < z < 1.5$ range, and some have moderately strong emission lines (Liu et al. 2000).

Two important open issues concern the surface density of EROs and the relative contribution of different classes of objects as a function of both color and apparent magnitude. We continue to lack statistically large samples of EROs. The most recent systematic large survey, by Thompson et al. (1999), covering an area of 154 arcmin^2, has yielded six

[1] Observatories of the Carnegie Institution of Washington, 813 Santa Barbara Street, Pasadena, CA 91101; lyan@ociw.edu.
[2] Physics and Astronomy Department, University of California, Los Angeles, CA 90095-1562.
[3] NASA Goddard Space Flight Center, Code 681, Greenbelt, MD 20771.
[4] NOAO Research Associate.
[5] *SIRTF* Science Center, Caltech, 770 South Wilson Avenue, Mail Stop 100-22, Pasadena, CA 91125.
[6] Cerro Tololo Inter-American Observatory, Casilla 603, La Serena, Chile.

TABLE 1

SELECTED NICMOS FIELDS

Field	R.A. (2000.0)	Decl. (2000.0)	b (deg)	T(F160W) (s)	$\mu(3\ \sigma)$ (mag arcsec^{-2})
0041+3302	00 41 16	33 02 04	−30	2040	25.0
0050−5200	00 50 12	−52 00 01	−65	2040	25.1
0049−5159	00 49 57	−51 59 57	−65	2040	25.1
0240−0140	02 40 01	−01 40 39	−54	2816	24.1
0240−0141a.....	02 40 07	−01 41 10	−54	2816	23.8
0240−0141b.....	02 40 12	−01 41 27	−54	2816	24.6
0354+0943	03 54 51	09 45 09	−32	1020	24.2
0354+0945	03 54 51	09 45 30	−32	1020	24.1
0457−0456	04 57 19	−04 56 51	−28	4480	25.7
0729+6915	07 29 57	69 15 02	29	5120	25.9
0741+6515	07 41 44	65 15 25	30	1030	24.9
1504+0110	15 04 37	01 10 31	49	510	23.4
1604+4318	16 04 55	43 18 56	48	3840	25.6
1631+3001	16 31 39	30 01 23	42	3584	25.1
1631+3730	16 31 40	37 30 30	43	3570	25.2
1631+3736	16 31 19	37 36 53	43	3570	24.9
1657+3526	16 57 23	35 26 05	37	18360	25.4
1940−6915	19 40 57	−69 15 04	30	6120	23.9
2044−3124	21 44 40	−31 24 55	37	2040	24.9
2220−2442	22 20 11	−24 42 14	56	5110	25.7
2325−2442	22 20 12	−24 42 00	−56	5120	25.9
2344−1524	23 44 00	−15 24 50	−70	3840	25.4

NOTE.—Units of right ascension are hours, minutes, and seconds, and units of declination are degrees, arcminutes, and arcseconds.

objects with $K \leq 19.0$ and $R-K > 6$. To quantify the fraction of different classes of EROs as a function of colors and magnitude, larger samples are required. The ERO surface density inferred from the Thompson et al. survey is 0.04 ± 0.016 arcmin^{-2} for $K \leq 19.0$ and $R-K > 6$. Depending on the K-band magnitude limit, $R-K$ color, and possibly environment, the reported surface densities of EROs range from 0.01 to 0.7 arcmin^{-2}, derived from several serendipitous surveys over small areas (Hu & Ridgway 1994; Cowie et al. 1994; Beckwith et al. 1998; Thompson et al. 1999). There have been suggestions that EROs tend to cluster particularly in regions around high-redshift active galactic nuclei compared with those around blank fields. The large luminosities and (admittedly uncertain) space densities imply that these objects represent a signficant constituent of the overall galaxy population and that their contribution to the overall rate of star formation is not negligible (e.g., Liu et al. 2000).

In this paper we present a sample of EROs discovered using NICMOS on the *HST* while operating in the parallel

TABLE 2

OPTICAL FOLLOW-UP OBSERVATIONS

Field	Inst.	Date	FWHM (arcsec)	$T(R)$ (s)	$\mu(3\ \sigma)$ (mag arcsec^{-2})
0041+3302.....	WIYN	1998 Nov 25	0.9	3600	26.9
0050−5200.....	LCO	1998 Oct 14	1.1	3500	26.8
0240−0141.....	CTIO	1998 Sep 15	1.2	2500	26.8
0354+0945.....	LCO	1998 Oct 12	0.8	4000	26.6
0457−0456.....	LCO	1998 Mar 02	0.8	3000	26.2
0729+6915.....	WIYN	1998 Nov 25	0.8	4800	26.9
0741+6515.....	WIYN	1999 Jan 18	0.7	3600	27.1
1504+0110.....	WIYN	1998 May 03	0.8	1800	25.8
1604+4318.....	WIYN	1998 May 02	0.7	3000	26.5
1631+3001.....	Keck	1999 May 21	0.7	900	27.3
1631+3001.....	WIYN	1998 Apr 27	0.7	3600	26.2
1631+3736.....	Keck	1999 May 21	0.6	300	26.5
1657+3526.....	Keck	1999 May 21	0.7	600	27.0
1940−6915.....	CTIO	1998 Sep 14	1.1	2500	26.8
2044−3124.....	LCO	1998 Oct 13	0.9	3500	26.7
2220−2442.....	LCO	1998 Oct 12	0.8	5400	27.1
2325−2442.....	WIYN	1998 Oct 24	0.8	1800	26.1
2344−1524.....	CTIO	1998 Sep 13	1.0	4000	26.9

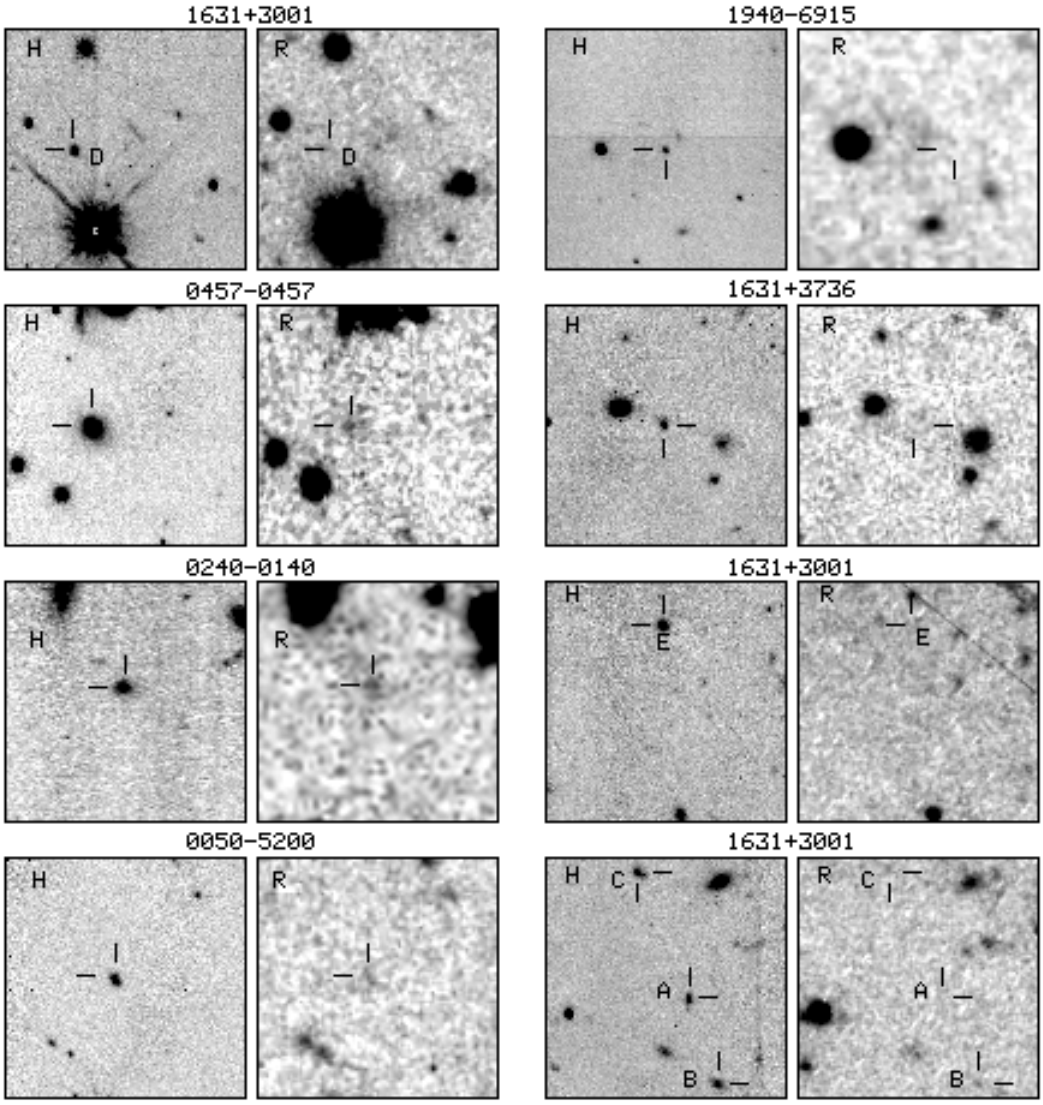

FIG. 1.—Images of EROs in the *R* and F160W bands

mode. Our combined NICMOS and optical survey covers only 16 arcmin^{-2}, but it provides high spatial resolution and a better signal-to-noise ratio in the near-IR than most ground-based surveys.

2. OBSERVATIONS AND REDUCTIONS

2.1. *Near-Infrared Images*

The images under discussion here were obtained with camera 3 on NICMOS (Thompson et al. 1998) using the F160W ($\lambda_c = 1.6$ μm, $\delta\lambda = 0.4$ μm) and F110W bandpasses ($\lambda_c = 1.1$ μm, $\delta\lambda = 0.8$ μm). The data were obtained in the parallel observing mode during the period from 1997 October to 1998 November, excluding the dedicated NICMOS camera 3 observing campaigns. This allowed us to observe fields that are essentially randomly distributed over the sky. The sensitivity varies from field to field because of different integration times and background levels. The NICMOS internal pupil adjustment mirror was set near the end of its travel, providing the best possible focus for camera 3. The point-spread function (PSF) in the images is slightly non-Gaussian, but it is well characterized by FWHM = 0.″25. We obtained four images per orbit, two each with the F110W and F160W filters. The field offset mirror was used to dither between two fixed positions 1.″8 apart in a direction aligned with one axis of the detector. In addition, small interorbit dither moves were executed for some of the pointings. The projected size of a camera 3 pixel is 0.″204, giving a 51″ × 51″ field of view for each image. A small area is lost in the construction of the final mosaic image. The NICMOS camera 3 parallel program covered approximately 200 arcmin^{-2} at high galactic latitude in its 14 months of operation. In the present work, we are limited by the amount and the depth of the visible-light data that we were able to collect for the NICMOS parallel fields. As described below, most of the NICMOS F160W images easily reach F160W magnitudes fainter than 21 (Vega magnitude) with high signal-to-noise ratios (eg. 20 σ at $H = 21.0$). Thus, to detect EROs at these depths requires 3 σ *R*-magnitude limits of 26 in our follow-up images. As the NICMOS camera 3 field of view is only 0.722 arcmin^{-2}, optical follow-up is quite inefficient.

We used McLeod's NicRed version 1.7 package (1997) to linearize and remove the cosmic rays from the MultiAccum images. Median images were derived from more than 50 pointings, and these were used to remove the dark and sky signals. Even with the optimal dark subtraction, there

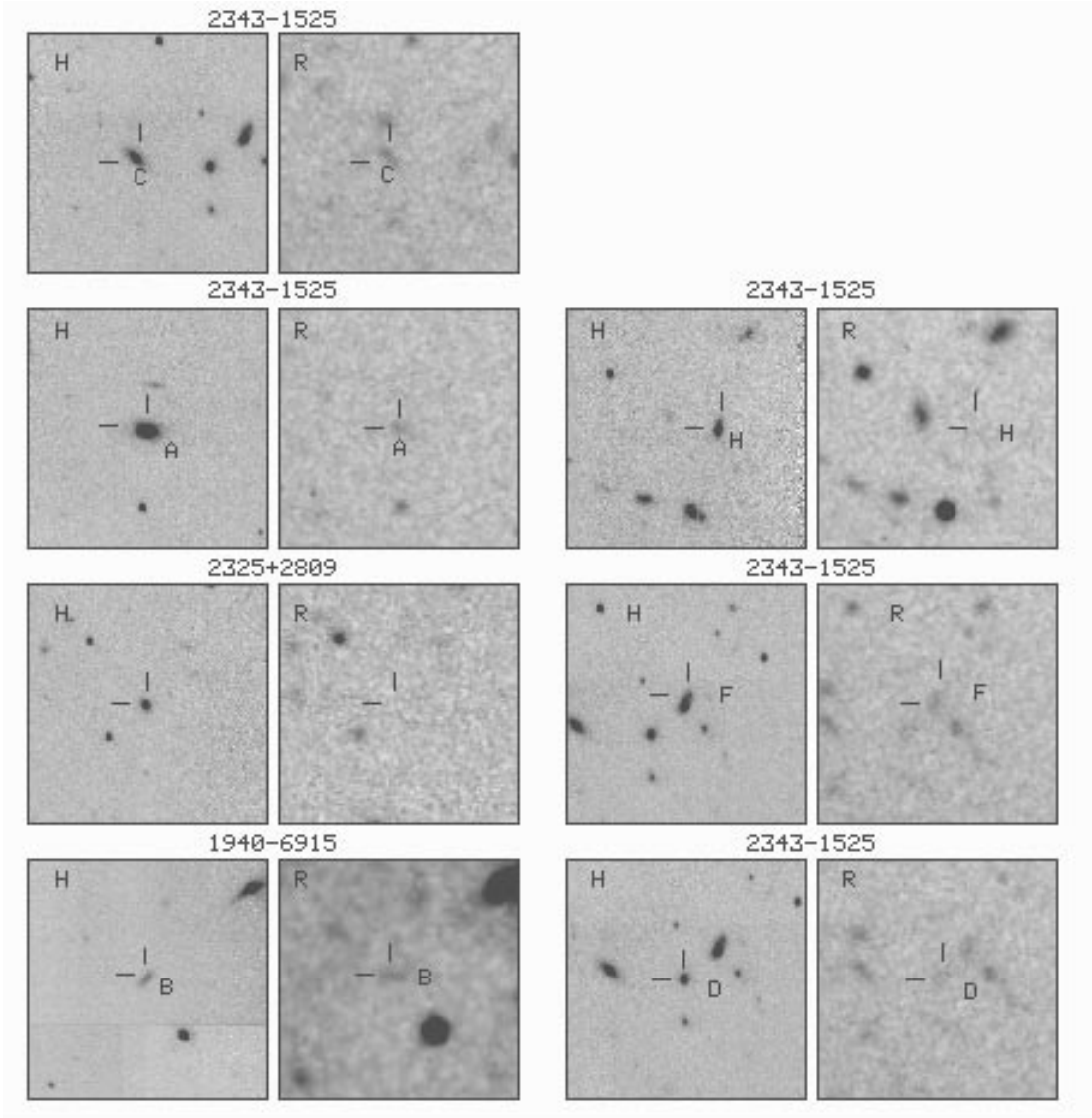

FIG. 1.—*Continued*

remain considerable frame-to-frame variations in the quality of the final images. The individual linearized, dark-corrected, flat-fielded, and cosmic-ray–cleaned images were shifted, masked, and combined to produce the final mosaic images. Before shifting, each image was 2×2 block–replicated and integer (0.″1) offsets were applied. In this way we avoided smoothing or interpolating the data. The Multi-Accum process is not 100% efficient in rejecting cosmic-ray events, and so we applied a 3 σ rejection when assembling the final mosaics. More details regarding the NICMOS imaging reduction can be found in the work of Yan et al. (1998).

In Table 1, we list 3 σ surface brightness limits in the F160W filter for the fields for which we have obtained optical data. The 50% completeness depth in the shallowest field is approximately $m(\mathrm{F160W}) = 22$. Thus our near-IR catalog is 100% complete at the ERO selection limit (F160W $\sim$ 21.5, as described below). We emphasize that our ERO search is entirely limited by the depth of the optical images.

2.2. *Optical Observations*

Multicolor CCD observations of several of the NICMOS parallel fields were made at Cerro Tololo Inter-American Observatory (CTIO), Las Campanas Observatory (LCO), WIYN observatory, Palomar Observatory, and the W. M. Keck Observatory. The date of the observations, duration of the *R* images, FWHM of the seeing, and 3 σ limiting surface brightness of the *R* images are listed in Table 2. The pixel scales range from 0.″2 for the LCO, WIYN, and Keck cameras to $\sim$0.″4 for the CTIO BTC Big Throughput Camera camera system. Several of the fields were observed on more than one occasion and from different sites to obtain photometric calibration. The seeing was better than 1″ for most of the fields. The data were reduced and calibrated using standard methods. The resulting images were interpolated and rotated to match the NICMOS fields, and true color images were constructed from the F160W, F110W, and *R* images (or F160W, *R*, and *V* when possible). This allowed for easy and efficient identification of objects with red colors. The photometry was performed on the original uninterpolated images.

3. RESULTS

3.1. *ERO Detection and Photometry*

All of the ERO identifications were made visually from comparisons between the aligned near-IR and optical images. The small size of each NICMOS image (51″ $\times$ 51″),

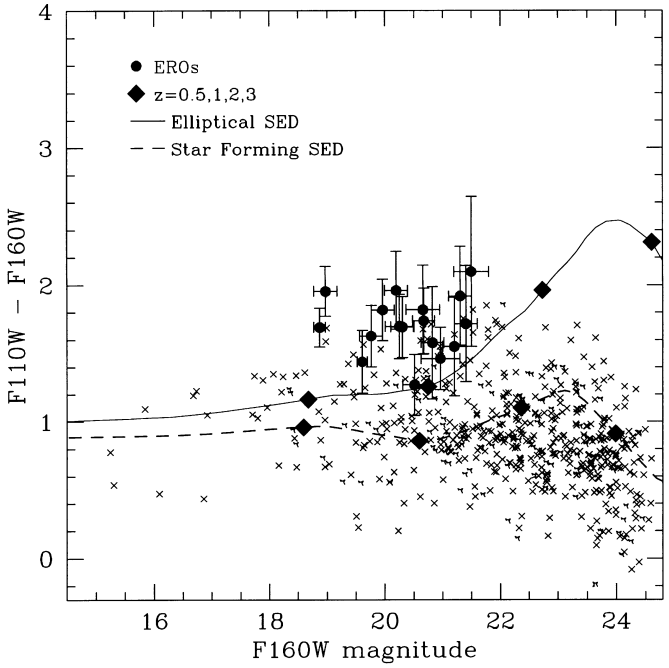

FIG. 2.—Infrared color-magnitude diagram for galaxies detected in 19 NICMOS fields, showing the EROs listed in Table 3 (*circles*) and synthetic color-magnitude tracks for an old elliptical galaxy (*solid line*) and a star-forming galaxy (*dashed line*), using the Bruzual & Charlot model. Diamonds indicate the places where redshifts are equal to 0.5, 1., 2., and 3. Here we assume $H_0 = 70$ km s^{-1} Mpc^{-1} and $q_0 = 0.1$. The error bars on the X- and Y-axes are $\pm 1\,\sigma$, calculated from SExtractor.

as well as its sensitive depth, made visual selection efficient. All of the EROs are well detected in the near-IR bands and were either undetected or marginally detected in the R-band images. The $R-$F160W colors were measured for all of the ERO candidates using the original uninterpolated images. The colors are subject to significant uncertainties because of the low signal levels of the red objects in the R-band images. The mismatch between the PSFs of NICMOS and ground-based CCD images adds a significant complication to the color measurement. We adopted the following method to estimate the $R-$F160W colors. We smoothed our F160W images to the same FWHM as the corresponding optical images. The F160W and R magnitudes were then measured in identical apertures. The aperture diameter is 2.5 times the measured FWHM in the R-band images. We used the SExtractor software (Bertin & Arnouts 1996) to measure the magnitudes.

In Table 3 we list the magnitudes of EROs in a variety of filters. These are isophotal magnitudes measured out to 1 σ isophotal radius. As our sample of EROs is well detected at F160W, isophotal magnitudes are a good measure of total magnitudes. For the EROs that are undetected in the optical images, their 3 σ magnitude limits within a 2.5 FWHM diameter aperture are used.

3.2. *Surface Density*

In a total of 22 NICMOS fields, covering 16 arcmin^{-2}, we detect 15 objects with $R-$F160W > 5. Table 3 lists their equatorial coordinates, near-IR and optical magnitudes, and optical-IR colors. For some fields, we also have K-band images taken with the Near-Infrared Camera (Matthews & Soifer 1994) on the Keck telescope (Teplitz et al. 1998). The ERO sample is selected with $R-$F160W > 5 and without any limits set on H magnitudes. Our color selection system is similar to the $R-H$ system used in ground-based observations, and so direct comparisons are possible.

Figure 1 shows the R- and F160W band images of each ERO. All of our EROs are resolved in the NICMOS camera 3 images and appear to be extended, except ERO 1940-6915A. This object has m(F160W) = 20.6 and appears to be unresolved in our NIC3 image. The remaining objects exhibit both elliptical and indeterminate morphologies. The detailed analyses of the ERO luminosity profiles using both the NICMOS camera 2 and camera 3 data will be presented in Yan & McCarthy (2000).

TABLE 3

EROs IN THE NICMOS PARALLEL FIELDS

Name	R.A. (J2000.0)	Decl. (J2000.0)	$R-K$	$R-H$	K	H	J	I	R	V	B
0050−5200A	00 50 13.176	−52 00 12.62	...	> 5.2	...	20.6	22.4	> 23.8	> 25.9	> 25.6	...
0240−0140A	02 40 06.780	−01 41 40.76	...	5.1	...	19.2	20.9	...	24.3	> 26.5	> 26.3
0457−0457A	04 57 20.184	−04 57 12.46	6.6	6.0	18.17	18.8	20.5	23.2	24.8	> 25.0	
1631+3001A	16 31 39.180	+30 01 19.60	...	> 5.3	...	21.4	23.1	...	> 26.9	...	...
1631+3001B.....	16 31 38.885	+30 01 26.33	...	> 5.6	...	21.3	23.2	...	> 26.9	...	...
1631+3001C	16 31 39.609	+30 01 09.42	...	> 5.5	...	21.2	22.7	...	> 26.9	...	...
1631+3001D	16 31 38.197	+30 01 01.51	...	> 6.1	...	20.8	22.3	...	> 26.9	...	...
1631+3001E.....	16 31 40.741	+30 00 49.19	...	> 6.3	...	20.3	22.0	...	> 26.9	...	...
1631+3736A	16 31 19.549	+37 37 01.08	...	5.0	...	21.4	23.6	...	25.0	...	...
1940−6915A	19 40 55.732	−69 15 17.82	...	> 5.2	...	20.6	22.6	...	> 25.7	> 25.1	> 26.0
1940−6915B.....	19 40 57.821	−69 15 07.40	...	> 5.2	...	20.5	22.2	...	> 25.7	> 25.1	> 26.0
2325+2809A	23 25 01.830	+28 09 25.30	...	> 5.3	...	20.2	22.2	...	> 25.5	...	...
2344−1525A	23 43 58.504	−15 25 12.74	6.1	5.0	17.8	18.9	20.8	...	23.9	25.6	> 26.2
2344−1525C[a].....	23 43 58.675	−15 24 56.33	5.6	4.4	18.7	19.9	21.5	...	24.3	24.6	> 26.2
2344−1525D	23 43 59.103	−15 24 57.42	> 5.8	> 5.0	19.5	20.5	21.8	...	> 25.4	> 25.6	> 26.2
2344−1525F[a].....	23 43 59.254	−15 25 00.63	5.9	4.5	18.2	19.7	21.4	...	24.1	24.2	24.9
2344−1525H	23 44 01.113	−15 25 10.83	> 6.2	> 5.2	19.1	20.2	21.9	...	> 25.4	> 25.6	> 26.2

[a] The $R-H$ colors for these two galaxies are slightly less than 5, but since they belong to the same cluster group, we included them for completeness. These two objects are excluded in the ERO surface density calculation.

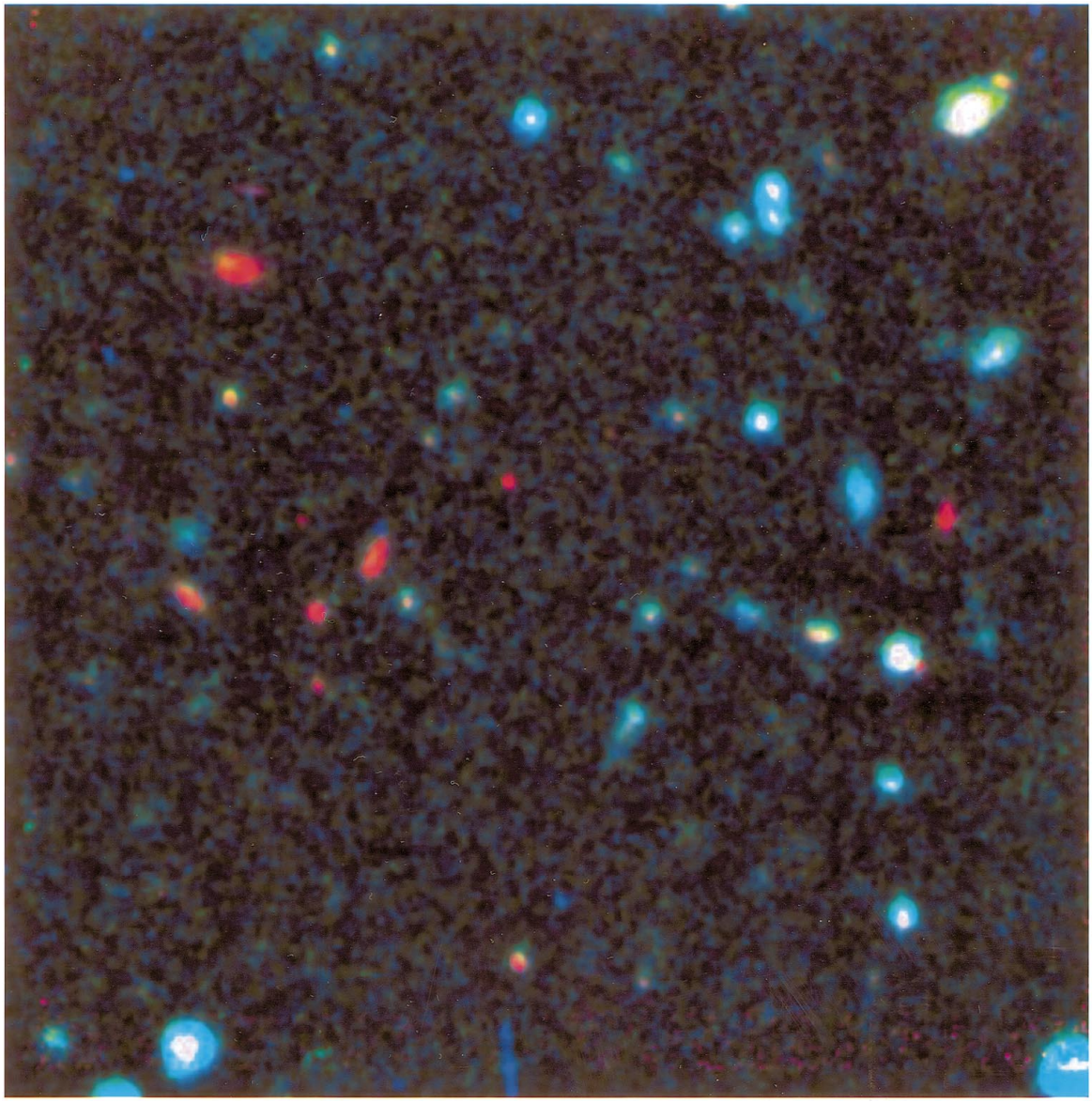

FIG. 3.—VR F160W composite color image of 2344−1524 field. The field shown here has size 50″ × 50″. The color image indicates a cluster of EROs.

In a few fields for which we have very deep optical images taken with the Low Resolution Imaging Spectograph (Oke et al. 1995) at the 10 m Keck telescope, we were able to find EROs with H magnitudes as faint as 21.4. The surface density of EROs depends on the magnitude limit of the sample. Including the two apparent clusters of EROs and the point source–like object ERO 1940-6915A, we estimate surface densities of 0.19 ± 0.11, 0.19 ± 0.1, 0.50 ± 0.18, and 0.94 ± 0.24 arcmin^{-2} for EROs with $R-\mathrm{F160W} > 5$ and F160W less than 19.5, 20.0, 20.5, and 21.5, respectively. If we exclude the two ERO clusters and the possible stellar object, the inferred surface density is significantly lower, 0.13 ± 0.08, 0.13 ± 0.08, 0.25 ± 0.13, and 0.38 ± 0.15 arcmin^{-2} for EROs brighter than 19.5, 20, 20.5, and 21.5, respectively. Here we did not include 2344−1525C and 2344−1525F, whose $R-H$ colors are slightly less than 5. Since our areal coverage is very small, the statistical errors in these estimates are large, particularly at bright magnitudes. If EROs have F160W$-K$ colors of 0.5–1, as suggested by our observations, our surface density estimate is consistent within 3 σ with that inferred from the ground-based ERO survey by Thompson et al. (1999), 0.04 ± 0.016 arcmin^{-2} for $R-K > 6$ and $K < 19$.

3.3. *Infrared Colors*

In Figure 2, we present F110W−F160W colors for all of the galaxies detected in 19 NICMOS fields, where we have both F160W and F110W images, as well as ground-based optical follow-up observations (see Table 1). Circles in the figure represent the EROs listed in Table 3. Overlaying on the data are color-magnitude tracks for a passively evolving L^* elliptical galaxy formed at $z = 10$ in a single burst lasting 1 Gyr and for a star-forming galaxy with constant star formation rate 1 $M_\odot$ yr^{-1}. Here we adopt $H_0 = 70$ km s^{-1} Mpc^{-1} and $q_0 = 0.1$. Diamonds indicate the places with redshifts of 0.5, 1, 2, and 3. The error bars on F110W−F160W colors and F160W magnitudes are ± 1 σ, calculated from SExtractor (Bertin & Arnouts 1996). The F110W−F160W colors of our $R-$F160W selected EROs appear to be redder than the average color of field galaxies (Fig. 2). They also appear to be redder than the $z \sim 0.9$ cluster elliptical population studied by Stanford, Eisen-

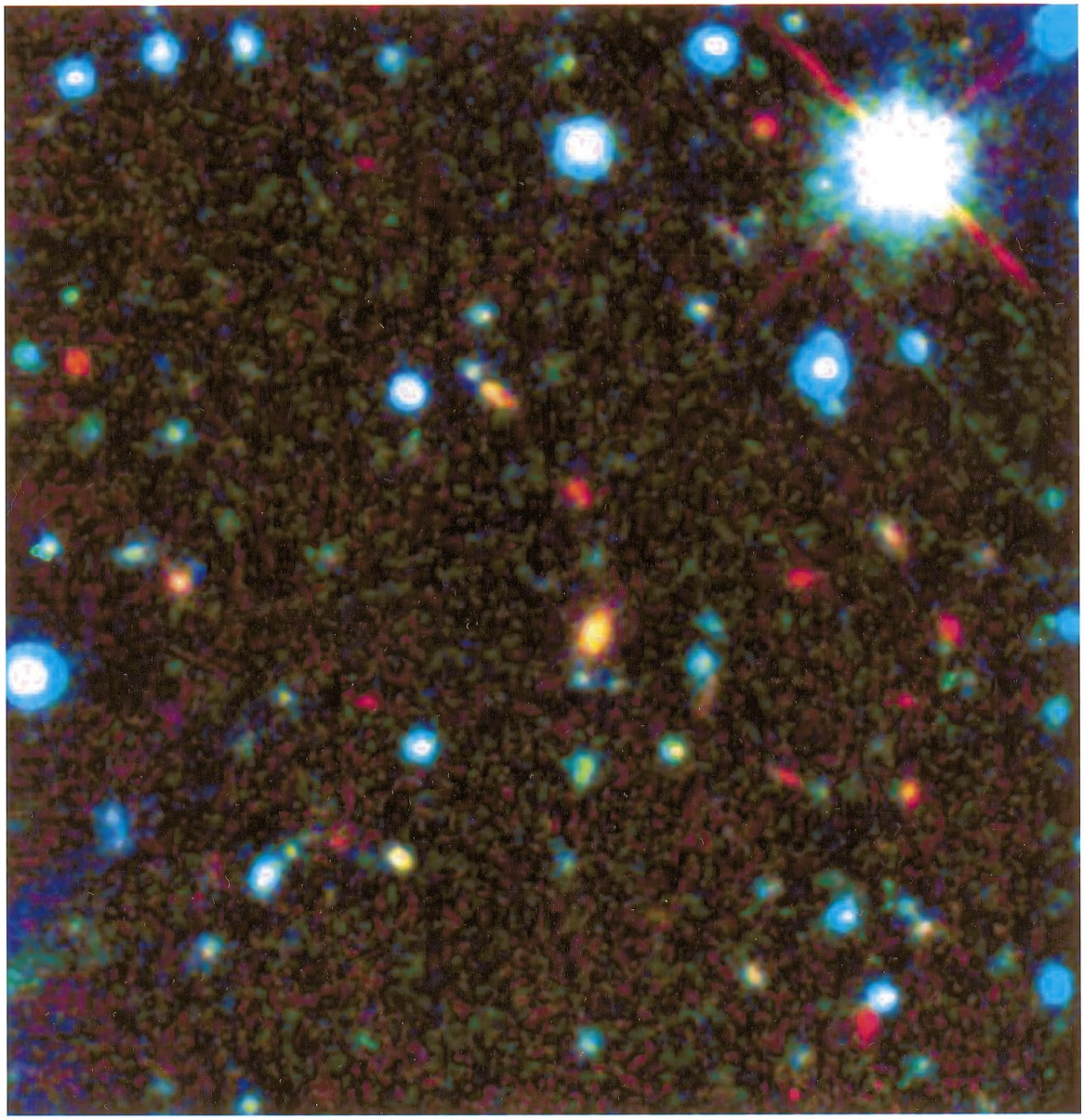

FIG. 4.— VR F160W composite color picture of 1631+3001 field showing a cluster of EROs. The field size is the same as in Fig. 3.

hardt, & Dickinson (1998; $J-H \sim 1.1$). There are some objects that have red $J-H$ colors, but their $R-H$ colors do not meet our ERO definition. These objects may contain small amounts of current star formation. If the objects in our ERO sample have luminosities near L^*, the median redshift of our sample is ~ 1, and the total range sampled is roughly $0.6 < z < 1.5$.

Among the 22 NICMOS pointings for which we have deep optical photometry we found two fields that each contain more than three objects meeting our ERO definition. Figures 3 and 4 show the VR F160W composite true color pictures of the ERO groups in 2344−1524 and 1631+3001, respectively. In the 2344−1524 field, we also obtained K-band images and the selected ERO candidates have $R-K \gtrsim 6$. The 1631+3001 field has many red objects, including several very faint objects with $F(160W) > 21.5$, which are not selected in our ERO sample. Figures 3 and 4 clearly indicate two potential groups or clusters of EROs. Follow-up spectroscopy is important for determining the cluster redshifts and the physical nature of these EROs. Our detections of two clusters of EROs over the small area ~ 16 arcmin^{-2} suggest that EROs tend to be strongly clustered. Previous studies by McCarthy et al. (1992) and Thompson et al. (1999) have also noted the ERO-clustering phenomenon from small statistical samples. Obviously, solving the problem of ERO clustering will be an important goal for future deep infrared surveys covering large areas.

We thank the staff of the Space Telescope Science Institute (STScI) for their efforts in making this parallel program possible. In particular, we thank Duccio Machetto, Peg Stanley, Doug van Orsow, and the staff of the PRESTO division. We also thank John Mackenty and members of the STScI NICMOS group for crafting the exposure sequences. Some of the data presented herein were obtained at the W. M. Keck Observatory, which is operated as a scientific partnership among the California Institute of Technology, the University of California, and the National

Aeronautics and Space Administration. The observatory was made possible by the generous financial support of the W. M. Keck Foundation. This research was supported, in part, by grants from the Space Telescope Science Institute, GO-7499.01-96A, AR-07972.01-96A, and PO423101. H. I. T. acknowledges funding by the Space Telescope Imaging Spectrograph Instrument Definition Team through the National Optical Astronomy Observatories and by the NASA Goddard Space Flight Center.

REFERENCES

Beckwith, S. V. W., Thompson, D., Mannucci, F., & Djorgovski, S. G. 1998, ApJ, 504, 107
Bertin, E., & Arnouts, S. 1996, A&AS, 117, 393
Cimatti, A., Andreani, P., Rottgering, H., & Tilanus, R. 1998, Nature, 392, 895
Cowie, L. L., Gardner, J. P., Hu, E. M., Songaila, A., Hodapp, K. W., & Windhorst, R. J. 1994, ApJ, 434, 114
Dey, A., Graham, J., Ivison, R. J., Smail, I., Wright, G. S., & Liu, M. C. 1999, ApJ, 519, 610
Dey, A., Spinrad, H., & Dickinson, M. 1995, ApJ, 440, 515
Dunlop, J., Peacock, J., Spinrad, H., Dey, A., Jimenez, R., Stern, D., & Windhorst, R. 1996, Nature, 381, L13
Elston, R., Rieke, M. J., & Rieke, G. H. 1988, ApJ, 331, L77
Graham, J. R., & Dey, A. 1996, ApJ, 471, 720
Hu, E. M., & Ridgeway, S. E. 1994, AJ, 107, 1303
Liu, M. C., Dey, A., Graham, J. R., Bundy, K. A., Steidel, C. C., Adelberger, K., & Dickinson, M. E. 2000, AJ, 119, 2556
Matthews, K., & Soifer, B. T. 1994, in Infrared Astronomy with Arrays: The Next Generation, ed. I. McLean (Dordrecht: Kluwer), 239
McCarthy, P. J., Persson, S. E., & West, S. C. 1992, ApJ, 386, 52
McLeod, B. 1997, in The 1997 *HST* Calibration Workshop, ed. S. Casertano, R. Jedrzejewski, C. D. Keyes, & M. Stevens (Baltimore: STScI), 281
Oke, J. B., et al. 1995, PASP, 107, 375
Soifer, T., et al. 1994, ApJ, 420, L1
Soifer, T. B., Matthews, K., Neugebauer, G., Armus, L., Cohen, J. G., Persson, S. E., & Smail, I. 1999, AJ, 118, 2065
Smail, I., Ivison, R. J., Blain, A. W., & Kneib, J.-P. 1998, ApJ, 507, L21
Smail, I., Ivison, R. J., Kneib, J.-P., Cowie, L. L., Blain, A. W., Owen, F. N., & Morrison, G. E. 1999, MNRAS, 308, 1061
Stanford, S. A., Eisenhardt, P. R., & Dickinson, M. 1998, ApJ, 492, 461
Teplitz, H. I., Gardner, J. P., Malumuth, E. M., & Heap, S. R. 1998, ApJ, 507, 17L
Thompson, D., et al. 1999, ApJ, 523, 100
Thompson, R. I., Rieke, M., Schneider, G., Hines, D. C., & Corbin, M. R. 1998, ApJ, 492, L95
Yan, L., & McCarthy, P. J. 2000, in preparation
Yan, L., McCarthy, P. J., Storrie-Lombardi, L. J., & Weymann, R. J. 1998, ApJ, 507, L19